Bifurcations and chaos in large Prandtl-number Rayleigh-Bénard Convection

Supriyo Paul,[1,*] Pankaj Wahi,[2,†] and Mahendra K. Verma[1,‡]

[1]*Department of Physics, Indian Institute of Technology, Kanpur 208 016, India*

[2]*Department of Mechanical Engineering,*
Indian Institute of Technology, Kanpur 208 016, India

(Dated: October 9, 2009)

Abstract

A low-dimensional model of large Prandtl-number (P) Rayleigh Bénard convection is constructed using some of the important modes of pseudospectral direct numerical simulations. A detailed bifurcation analysis of the low-dimensional model for $P = 6.8$ and aspect ratio of $2\sqrt{2}$ reveals a rich instability and chaos picture: steady rolls, time-periodicity, quasiperiodicity, phase locking, chaos, and crisis. Bifurcation analysis also reveals multiple co-existing attractors, and a window with time-periodicity after chaos. The results of the low-dimensional model matches quite closely with some of the past simulations and experimental results where they observe chaos in RBC through quasiperiodicity and phase locking.

PACS numbers: 47.20.Bp, 47.20.Ky, 47.52.+j

*Electronic address: supriyo@iitk.ac.in

†Electronic address: wahi@iitk.ac.in

‡Electronic address: mkv@iitk.ac.in

I. INTRODUCTION

Rayleigh Bénard convection (RBC) exhibits a host of complex phenomena. Instabilities, patterns, and chaos are observed near the onset of convection, while turbulence is seen far beyond the onset [1]. Bifurcation diagrams are often used to study instabilities and chaos. In this paper we report a bifurcation analysis for large-Prandtl number RBC flow obtained using a low-dimensional model.

The two most important parameters for RBC are the Rayleigh number R (ratio of buoyancy and dissipative force) and the Prandtl number P (ratio of viscosity and thermal diffusivity). Convection starts at the critical Rayleigh number R_c, which is independent of P. For non-zero Prandtl number, the primary instability at the onset of convection is always in the form of two-dimensional (2D) straight rolls [2]. These rolls become unstable through secondary instabilities, and they bifurcates into a sequence of dynamic patterns [3, 4, 5]. Some examples of the resulting patterns are squares and hexagons, asymmetric patterns, oscillating patterns, relaxation oscillations of rolls and squares, etc. [6].

The sequence of instabilities and onset of chaos are quite different for low-Prandtl number (low-P) convection [7] and large-Prandtl number (large-P) convection [8, 9, 10, 11]. For low-P convection, the 2D rolls become unstable close to the onset and wavy rolls are generated through secondary instabilities, thus making the flow three-dimensional (3D). These bifurcations and route to chaos for low-P and zero-Prandtl (zero-P) number convection have been studied extensively (see [1, 12, 13] and references therein). The scenario however is quite different for large-P convection. The secondary instabilities are delayed here, and the 2D rolls continue to be solutions till larger Rayleigh numbers. It has been reported that 2D convection results have significant similarities with 3D results for large-P convection [14, 15]. We exploit this observation to analyze bifurcation and chaos for large-P convection using a low-dimensional model containing only 2D modes. A major advantage of this simplification is that the number of modes required for 2D convection is much fewer than 3D convection, thus enabling the bifurcation analysis.

Krishnamurti [16] performed extensive convection experiments on mercury ($P \approx 0.02$), air ($P \approx 0.7$), water ($P \approx 6.8$), freon 113 ($P \approx 7$), and silicon oil ($P \sim 100$). She studied transition from 2D convection to 3D convection and subsequent generation of oscillatory, chaotic, and turbulent convection. Busse and Whitehead [3] also reported 'zigzag instability'

and 'cross-roll instability' in an experiment on silicon oil.

Libchaber *et al.* [7] studied the routes to chaos for RBC in mercury (a low-P fluid) as a function of R and the applied mean magnetic field; at different values of the parameters they observed chaos through various routes: period doubling, quasiperiodic, and soft instability. Gollub and Benson [10] studied route to chaos in RBC of water at two different Prandtl numbers, $P = 2.5$ and 5, for different aspect ratios Γ and observed very rich behaviour. For $P = 5$ and $\Gamma = 3.5$ they observed steady rolls till $r = R/R_c = 27.2$ (r is called 'reduced Rayleigh number'), at which point periodic flow starts. At $r = 32$, a second frequency appears in the system and the flow becomes quasiperiodic. Phase locking occurs at $r = 44.4$ that finally leads to chaos at $r = 46.0$. Gollub and Benson also observed period doubling route to chaos for $P = 2.5$ and $\Gamma = 3.5$, and quasiperiodic route to chaos with the third frequency for $P = 5$ and $\Gamma = 2.4$. They also observed intermittency in their system.

In another experiment, Maurer and Libchaber [17] observed frequency locking and subsequent generation of chaos in liquid helium as a result of generation of new frequency modes. Giglio *et al.* [8] observed period-doubling route to chaos in their convective experiment on water. Bergé et al. [9] found intermittency in RBC of silicon oil. Ciliberto and Rubio [18] reported localized oscillations and travelling waves in RBC. Morris *et al.* [19] discovered spatio-temporal chaos in RBC of silicon oil. These results indicate complex nonlinear dynamics including chaos in RBC.

Direct numerical simulation (DNS) of 2D and 3D RBC have been used to study various convective states including turbulence. Curry *et al.* [20] performed detailed 3D DNS for $P = 10$ under free-slip boundary conditions; they reported steady convection till $r \approx 40$, after which single frequency oscillations are observed till $r \approx 45$. Subsequently they observed quasiperiodicity ($r \approx 45 - 55$), phase locking ($r \approx 55 - 65$), and chaos ($r > 65$). Yahata [21] performed DNS using finite difference scheme (MAC method) on no-slip boundary condition for $P = 5$, $\Gamma_x = 3.5$ and $\Gamma_y = 2$. The results show a series of bifurcations from monoperiodic $\rightarrow$ biperiodic $\rightarrow$ frequency-locked state $\rightarrow$ chaotic state. Mukutmoni and Yang [22] reported a numerical study of RBC in a rectangular enclosure with insulated sidewalls. They observed a period-2 response after a periodic solution but the route to chaos is through quasiperiodicity. However, on imposing symmetry of the velocity and temperature field about the mid-planes, they observed a period-doubling route to chaos. They have also reported periodic solutions after chaos.

In two dimensions, Moore and Weiss [23] simulated $P = 6.8$ RBC using a spectral method with free-slip boundary conditions; they studied heat transport as a function of the Rayleigh number. McLaughlin and Orszag [24] considered RBC in air ($P = 0.71$) with no-slip boundary conditions; they obtained periodic, quasiperiodic, and chaotic states for Rayleigh numbers between 6500 and 25000. Curry *et al.* [20] performed detailed DNS for $P = 6.8$ fluid in 2D and observed oscillations with a single frequency at $r \approx 50$, and with two frequencies at $r \approx 290$. They also reported weak chaos beyond $r = 290$, and a periodic solution after $r \approx 800$. Goldhirsch *et al.* [25] also simulated 2D RBC and observed complex behaviour.

Recently, Paul *et al.* [26] performed 2D DNS for free-slip boundary condition for a large range of Rayleigh numbers and obtained steady convection ($r = 0 - 80$), periodicity ($r = 80 - 660$), quasiperiodicity ($r = 660 - 770$), and chaos ($r = 770 - 890$). They also observed periodic and steady convection beyond the chaotic state. Paul *et al.* [26]'s results are in general agreement with those of Curry *et al.* [20] and Goldhirsch *et al.* [25] with some difference in the Rayleigh numbers. One noticeable difference between 2D RBC and 3D RBC is that the secondary instabilities in 2D RBC occur at significantly higher values of r than those in 3D RBC.

The origin of various convective patterns and chaos in DNS is not apparent due to various interactions among the large number of modes. Rather, they have been analyzed using low-dimensional models of RBC. Curry [27] constructed a 14-mode model of RBC with a small amplitude periodic modulations in the heat equation. He observed chaos for $P = 10$. The low-dimensional model of Curry shows features similar to the experiments of Gollub and Benson [10] namely periodicity, quasiperiodicity, and chaos. Curry [28] also studied the 14-mode model without any modulation, and compared its results with those from the Lorenz model.

Yahata [29] studied transition to chaos in RBC using a 48-mode system of equations under no-slip boundary conditions. For $P = 5$, $\Gamma_x = 2$ and $\Gamma_y = 3.5$, he obtained periodic $\rightarrow$ quasiperiodic motion with two fundamental frequencies $\rightarrow$ quasiperiodicity with three frequencies $\rightarrow$ chaos. The whole sequence of bifurcations occur in the range of $r = 39.77$ to 41.04. Yahata [30] continued the above analysis for $P = 2.5$ with the same aspect ratio and reported period-doubling route to chaos for r in the range of 24.46 to 29.35.

In the above work, Curry [27] and Yahata [29, 30] numerically integrate the low-dimensional models for certain r values and observe various patterns. Some of the short-

comings of this method are that it could miss the behaviour in narrow windows, and the bifurcation points cannot be precisely located. In the present paper we numerically time advance the fixed points, limit cycles, and chaotic attractors, which provides a much more detailed bifurcation picture than that obtained by studying patterns at selected r values. The approach in the present paper is very similar to a recent work by Pal *et al.* [13] where a detailed bifurcation diagram was constructed for zero-P convection using a 13-mode system; this system was obtained using the energetic modes of DNS. Note that in large-P convection chaos sets in at a much larger Rayleigh number than in low-P and zero-P convection. As a consequence, large-P convective flows contain a large number of energetic modes at the onset of chaos. A bifurcation analysis of these large number of modes is very difficult and impractical. To circumvent this difficulty we study 2D convection, which is not a serious limitation for large-P convection since 2D and 3D convection have significant similarities [14, 15].

We perform our low-dimensional analysis for $P = 6.8$, which is the Prandtl number of water, a representative of large-P fluid. A significant advantage of choosing this Prandtl number is that a large number of DNS and experiments have been performed for water. We find that optimal number of real Fourier modes of our low-dimensional model is 30. The convective patterns–steady, periodic, quasiperiodic, and chaotic rolls–observed in DNS and experiments are captured in our low-dimensional model.

The outline of the paper is as follows. In Section II we describe the governing equations and the low-dimensional model. Details of the various convective regimes, bifurcation scenario and route to chaos associated with this model is presented in section III. The last section contains discussions and conclusions.

II. THE LOW-DIMENSIONAL MODEL AND ITS NUMERICAL SIMULATION

In RBC, a thin layer of fluid is confined between two thermally conducting horizontal plates that are separated by a distance d. The fluid has kinematic viscosity ν, thermal diffusivity κ, and thermal expansion coefficient α. An adverse temperature gradient $\beta = \Delta T/d$ is imposed across the fluid layer, where ΔT is the temperature difference across the layer. We assume Boussinesq approximation for the fluid [1]. The relevant hydrodynamic equations are nondimensionalized using the length scale d, the large-scale velocity scale

$\sqrt{\alpha\beta g d^2}$, and the temperature scale ΔT to yield [1]

$$\partial_t \mathbf{v} + (\mathbf{v}\cdot\nabla)\mathbf{v} = -\nabla p + \theta\hat{z} + \sqrt{\frac{P}{R}}\nabla^2\mathbf{v}, \tag{1}$$

$$\partial_t \theta + (\mathbf{v}\cdot\nabla)\theta = v_3 + \frac{1}{\sqrt{PR}}\nabla^2\theta, \tag{2}$$

$$\nabla\cdot\mathbf{v} = 0, \tag{3}$$

where $\mathbf{v} = (v_1, v_2, v_3)$ is the velocity fluctuation, θ is the perturbations in the temperature field from the steady conduction state, $R = \alpha g\beta d^4/\nu\kappa$ is the Rayleigh number, $P = \nu/\kappa$ is the Prandtl number, g is the acceleration due to gravity, and $\hat{z}$ is the buoyancy direction.

The above equations are often solved using direct numerical simulation (DNS). One of the popular numerical technique is pseudospectral method in which the velocity and the temperature fields are expanded in the Fourier/Chebyshev basis. These numerical simulations have been able to reproduce various patterns, chaos, and turbulence observed in experiments. The convection simulations are however very expensive in terms of computer time and memory. Also a large number of modes present in DNS obscures the internal dynamics. A popular method to analyze such systems is a bifurcation analysis of appropriate low-dimensional systems. Using this technique we can study the origin of various patterns and chaos in RBC. For our low-dimensional model we choose fourteen complex modes and two real modes that represent the large-scale flow structures. Expansion of the vertical velocity field v_3 and the temperature field θ using these modes yields

$$\begin{aligned}
v_3(x,z,t) &= W_{101}(t)\exp(ik_c x)\sin(\pi z) + W_{103}(t)\exp(ik_c x)\sin(3\pi z) \\
&+ W_{105}(t)\exp(ik_c x)\sin(5\pi z) + W_{202}(t)\exp(2ik_c x)\sin(2\pi z) \\
&+ W_{301}(t)\exp(3ik_c x)\sin(\pi z) + W_{303}(t)\exp(3ik_c x)\sin(3\pi z) \\
&+ W_{501}(t)\exp(5ik_c x)\sin(\pi z) + c.c., \\
v_2(x,z,t) &= 0, \\
\theta(x,z,t) &= \theta_{101}(t)\exp(ik_c x)\sin(\pi z) + \theta_{103}(t)\exp(ik_c x)\sin(3\pi z) \\
&+ \theta_{105}(t)\exp(ik_c x)\sin(5\pi z) + \theta_{202}(t)\exp(2ik_c x)\sin(2\pi z) \\
&+ \theta_{301}(t)\exp(3ik_c x)\sin(\pi z) + \theta_{303}(t)\exp(3ik_c x)\sin(3\pi z) \\
&+ \theta_{501}(t)\exp(5ik_c x)\sin(\pi z) + c.c. \\
&+ \theta_{002}(t)\sin(2\pi z) + \theta_{004}(t)\sin(4\pi z)
\end{aligned} \tag{4}$$

where *c.c.* stands for the complex conjugate, and the three subscripts denote the Fourier wavenumber indices along x, y, and z directions respectively. These modes correspond to the free-slip boundary condition for the velocity modes. Note that $v_1(x,z)$ can be computed using the incompressibility condition $\nabla \cdot \mathbf{v} = 0$. We choose $k_c = \pi/\sqrt{2}$, hence the aspect ratio of our model is $2\sqrt{2}$. The Galerkin projection of Eqs. (1-3) on these modes yields a set of thirty coupled ordinary differential equations (ODEs) for the real and imaginary parts of the Fourier modes. These thirty nonlinear ODEs comprise our low-dimensional model.

The above modes represent two-dimensional rolls. It has been reported earlier that the 2D and 3D convection have significant similarity for large-P flows [15]. Therefore we expect our low-dimensional model to capture the dynamics of large-P convection. Our model with 2D rolls has 30 modes while a full 3D low-dimensional model would have many more modes that would make the bifurcation analysis of the model very difficult. Note that three-dimensional patterns like squares are not accessible to our model. However quasiperiodicity and the origin of chaos are expected to be common for both 2D and 3D convection for large Prandtl number flows.

Our low-dimensional model is quite similar to that of Curry [27]. A major difference is that in our model all the modes except θ_{002} and θ_{004} are complex in contrast to Curry's model in which they are all real. Also, we keep the mode (105), whereas Curry keeps (204). Several of the patterns and chaos reported in the experiments of Gollub and Benson [10] have been observed by Curry when he includes small amplitude modulation. We do not require any modulation or any additional forcing (other than buoyancy) in our model to produce these patterns and chaos. Yahata [29, 30] studied RBC under no-slip boundary condition by expanding the velocity and temperature fields using mixed basis functions (Chebyshev along the buoyancy direction and Fourier along the horizontal directions) and observed similar behaviour. Surprisingly the patterns and chaos reported for the no-slip and the free-slip boundary conditions are quite similar.

We numerically solve the low-dimensional model using random initial conditions. In our low-dimensional model, we observe various patterns: steady convection, periodicity, quasiperiodicity, and chaos at different values of Rayleigh numbers (see Fig. 1). Figure 1) also shows that the system becomes periodic after chaos, and then it becomes chaotic again.

A curious feature of our model is that for the periodic solutions ($r = 27.6 - 40.3$), the

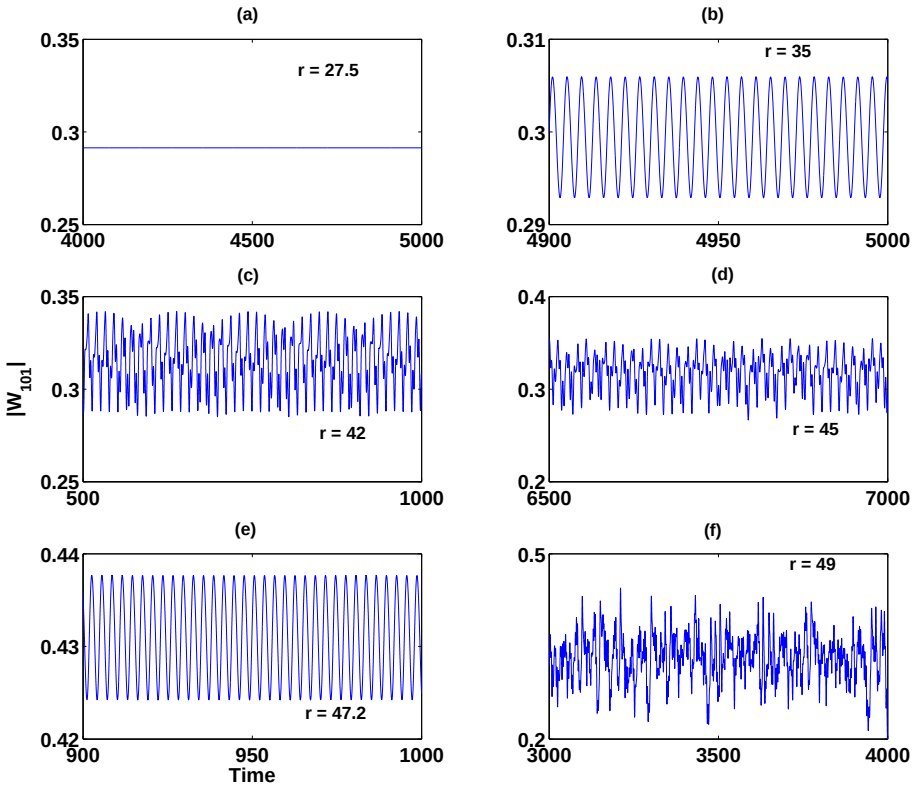

FIG. 1: Time series of the amplitude of the complex mode W_{101} generated by the low-dimensional model at various representative reduced Rayleigh numbers (r). We observe (a) steady convection ($r = 27.5$), (b) time-periodic convection ($r = 35$), (c) quasi-periodicity ($r = 42$) and (d) chaos ($r = 45$). Subsequently, (e) a window of time-periodic state ($r = 47.2$) followed by (f) a chaotic state ($r = 49$) is observed.

frequency of the Fourier amplitude is twice that of its phase (see Fig. 2). This feature can also be understood using the bifurcation analysis that will be discussed below.

The origin of the observed patterns can be studied more rigorously using the bifurcation analysis which is the subject of the next section.

III. BIFURCATION ANALYSIS OF THE LOW-DIMENSIONAL MODEL

In Fig. 3 we present a bifurcation diagram obtained by numerical integration of the low-dimensional model for $P = 6.8$ and the aspect ratio of $2\sqrt{2}$. The reduced Rayleigh number

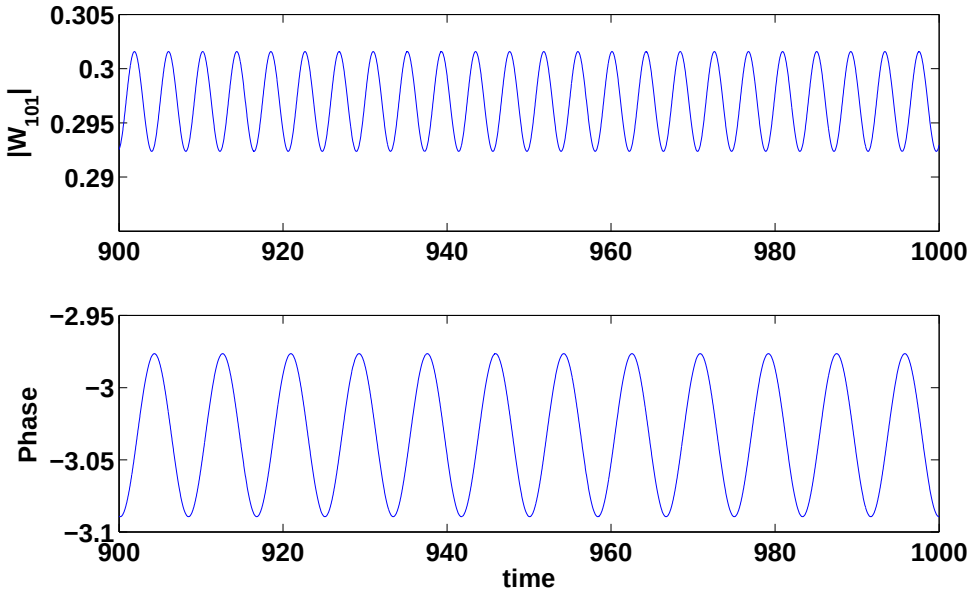

FIG. 2: Time-series of amplitude and phase of the complex W_{101} mode at $r = 30$. The amplitude oscillates at double the frequency of its phase.

r is the bifurcation parameter in our analysis. The unstable solutions have not been shown in Fig. 3. To generate this bifurcation diagram, numerical simulations have been performed with a fixed initial condition till $t = 20000$ (large-scale eddy turnover time). Transients till $t = 5000$ are eliminated and the extremum values of $|W_{101}|$ are plotted for later time. The stability and bifurcations of the steady states in this numerically generated bifurcation diagram are complimented by an eigenvalue analysis of the jacobian evaluated at the fixed points, and the eigenvalue of the associated Floquet matrix for the limit cycles. For this complimentary analysis, a fixed point is obtained numerically using the Newton-Raphson method for a given r, and the branches of the fixed points are subsequently obtained using a fixed arc-length based continuation scheme (similar to the analysis in Pal *et al.* [13]).

For $r < 1$, there is no convection in the system and heat is transported solely by conduction. The conduction state corresponds to the trivial fixed point of our system. At $r = 1$, the system undergoes a pitch-fork bifurcation and time-independent convection states are born as non-trivial fixed points. Note that there are two nonzero solutions near the onset of convection (e.g, $\pm W_{101}$). In Fig. 3 we plot $|W_{101}|$ vs. r. The new stable roll solutions (blue curve labeled 'FP') remain stable till $r \approx 27.6$.

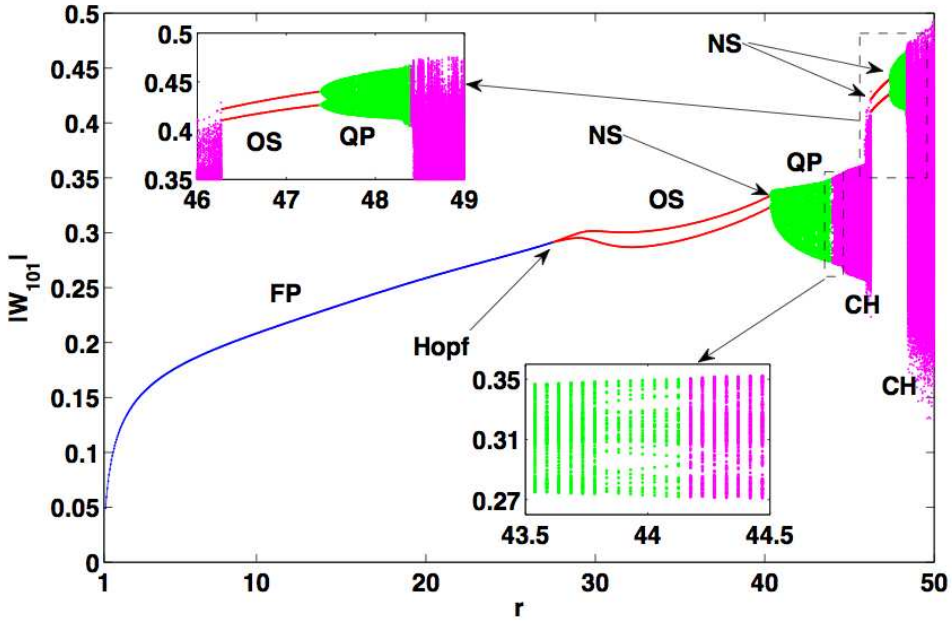

FIG. 3: Bifurcation diagram of the low-dimensional model representing large-Prandtl number RBC. 'FP' (blue curve) is the steady roll, 'OS' (red curve) is the time-periodic roll, 'QP' (green patch) is the quasi-periodic roll, and 'CH' (pink patch) is the chaotic state. 'NS' indicates the Neimark-Sacker bifurcation point. A window of periodic and quasiperiodic states is observed in the band of $r = 46.2 - 48.4$.

The branch of fixed points corresponding to the steady convective rolls undergoes a supercritical Hopf bifurcation at $r = 27.6$. As a consequence, the time-independent steady state solution becomes unstable and a new stable time-periodic state (limit cycle) is born. The limit cycle solution is shown as a red line with the label 'OS' in the bifurcation diagram (Fig. 3). The two lines of 'OS' state designate the maxima and minima of $|W_{101}|$ respectively. The time variation of the modes is however more complex. As shown in Fig. 2, the amplitude of the mode W_{101} vary with frequency twice that of its phase. This phenomena can be understood as follows. At the Hopf bifurcation point, the eigenvectors associated with the pair of purely imaginary eigenvalues $\pm i\omega$ have components only along the imaginary part of the Fourier modes (e.g., $\Im(W_{101})$). Hence, $\Im(W_{101})$ oscillates with the frequency ω corresponding to the Hopf point. The real parts of the Fourier modes are generated purely due to the quadratic nonlinearities involving products of two imaginary parts of the modes;

hence 2ω (superharmonic) is the leading frequency of the real parts and the amplitudes of modes.

We determine the stability of the above time-periodic state using the Floquet theory. We numerically construct the fundamental (Floquet) matrix associated with the time-periodic state and compute its eigenvalues (called 'Floquet multipliers'). All the Floquet multipliers for a stable limit cycle have magnitude less than one. For an unstable limit cycle, at least one of them has a magnitude greater than one. When the Floquet multipliers cross along the positive real axis, new limit cycles may appear or disappear ('pitchfork' or 'turning point' bifurcation). If they cross the negative real axis, the frequency of the limit cycle doubles in a 'period-doubling' bifurcation. However, a pair of complex-conjugate multipliers may also cross the unit circle in the complex plane, wherein another frequency is generated. This bifurcation is known as 'Niemark-Sacker' (NS) or a secondary Hopf bifurcation.

Fig. 4 illustrates the magnitude of the largest Floquet multiplier as a function of the reduced Rayleigh number r, while Fig. 5 shows the movement of the Floquet multipliers around several values of r. For these calculations, we proceed as follows. The limit cycle along with its time-period is obtained as a fixed point of an appropriately defined map (described in appendix A) using the Newton-Raphson method for a given r. The branch of limit cycles is subsequently computed using a fixed arc-length based continuation scheme. The fundamental matrix and the eigenvalues associated with the limit cycles for each value of r are then evaluated numerically.

Our computations reveal that the largest Floquet multiplier has magnitude less than one up to $r \approx 40.3$ (till 'A' in Fig. 4), hence the limit cycle (periodic orbit) remains stable till $r \approx 40.3$. The system undergoes a Niemark-Sacker (NS) near $r \approx 40.3$ as illustrated in Fig. 5(a). As a result of NS bifurcation, a second frequency (incommensurate with the first one) is generated, and the phase space trajectories show a transition from periodic orbits to quasiperiodic orbits. The quasiperiodic state is shown as a green patch labeled 'QP' in the bifurcation diagram (Fig. 3). The phase space trajectories in this regime lie on a torus as illustrated in Fig. 6(a) for $r = 42$. The power spectral density of the mode $|W_{101}|$ shown in Fig. 7(b) have two leading frequencies whose frequency ratio is is approximately 3.099. To identify the leading frequency, the power spectral density for the periodic state is shown in Fig. 7(a).

As the bifurcation parameter r is increased further, the two frequencies get phase locked

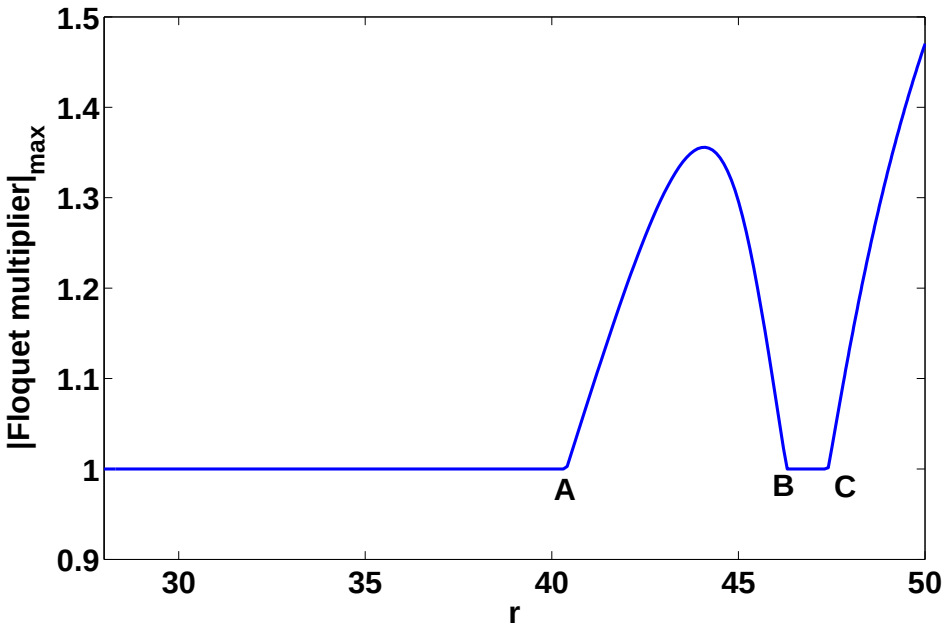

FIG. 4: The largest Floquet multiplier of the low-dimensional system as a function of r. The largest Floquet multiplier is greater than 1 beyond $r = 40.3$ (point 'A') except in the 'BC' window in which we observe periodic states.

to yield a periodic solution. This occurs in a narrow window in Fig. 3 and its lower inset. The phase space trajectories still lie on a torus but they form a periodic orbit as shown in Fig. 6(b) for $r = 44$. The time-period of this periodic orbit is approximately 150 non-dimensional time units, and the ratio of the two leading frequencies f_1/f_2 is approximately 3.152 ($\sim 167/53$). In Fig. 5(b) we show the movement of the Floquet multipliers in the phase locked region. During this movement of the largest Floquet multipliers the two frequencies get phase locked. The power spectrum of the mode W_{101} for the phase-locked state is illustrated in Fig. 7(c). Gollub and Benson [10] and Curry *et. al.* [20] report f_1/f_2 to be approximately 7/3 and 10/3 respectively for their phase-locked regime. Our $f_1/f_2 \approx 167/53$ is in general agreement with these earlier results.

With a further increase in the bifurcation parameter, the system becomes chaotic at around $r = 44.2$. The route to chaos is similar to that in Curry-Yorke model (§VIII.3 [31]) where chaos appears after quasiperiodicity in T^2 (2-Torus) and phase locking. In the bifurcation diagram (Fig. 3), the chaotic region is shown by colored pink patch labeled

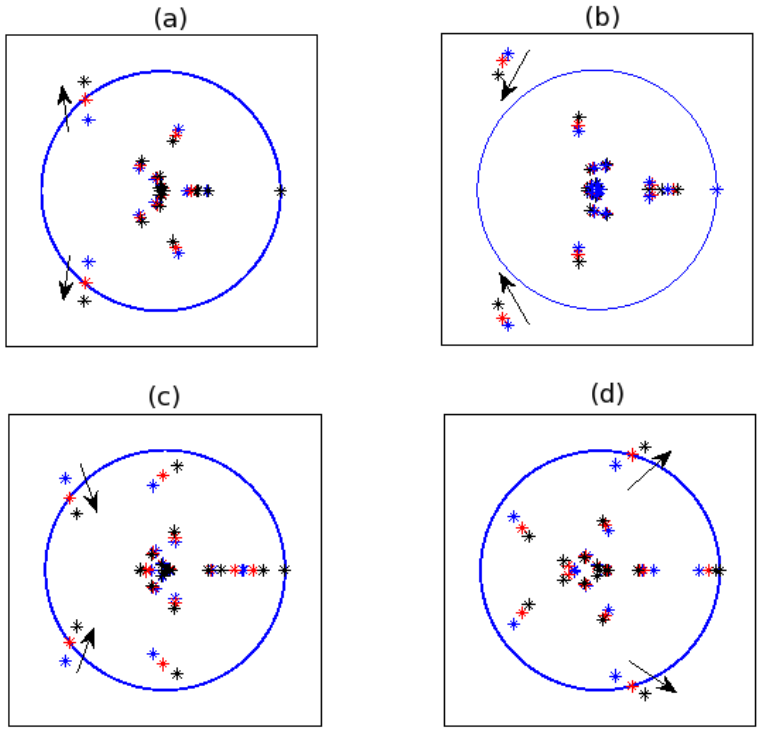

FIG. 5: Representation of the Floquet multiplier (FM) for various scenarios. Blue points indicate initial stage, red points indicate intermediate stage, and grey points indicate the final stage of the movement of the FM. (a) The FM crosses the unit circle through NS bifurcation creating a quasiperiodic state. (b) The motion of the FM during the phase-locked regime. Note that the largest FM remain outside the unit circle in this regime. (c) The largest FM moves into the unit circle resulting in a periodic solution. (d) The largest FM crosses the unit circle again creating a quasiperiodic solution.

as 'CH'. As shown in Fig. 7(d) the power spectrum of the mode W_{101} is broad indicating chaotic nature of the attractor. At around $r = 45.9$, the size of the chaotic attractor suddenly increases as a result of an 'interior crisis'. This feature is illustrated in Fig. 8 where we plot the phase space projection on the $|W_{101}| - |W_{103}|$ plane at $r = 45.8$ and $r = 45.9$.

The chaotic state described above exists till $r \leq 46.2$ after which we observe periodic solutions (the red curves in Fig. 3) that emerge from an inverse NS bifurcation. This inverse NS bifurcation is illustrated in Fig. 5(c) wherein the largest Floquet multipliers enters into the unit circle making the limit cycles stable. This stable time-periodic orbit continues till

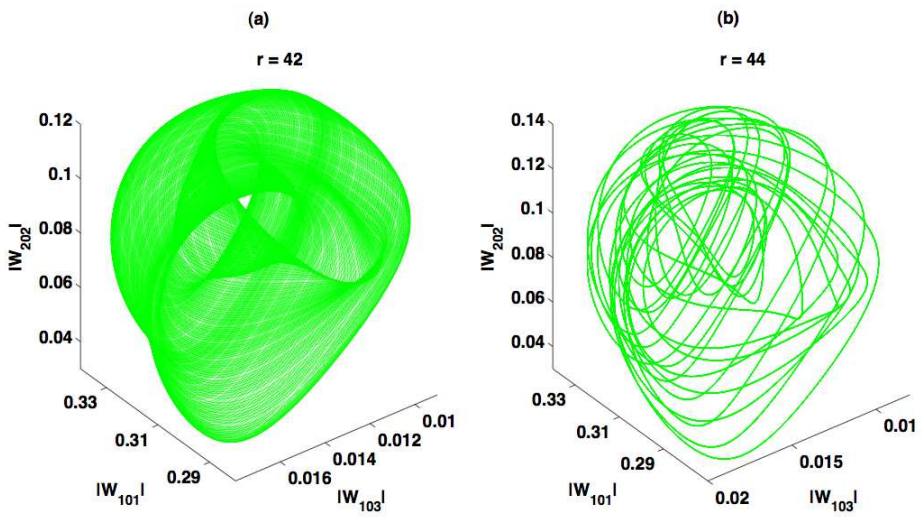

FIG. 6: A three-dimensional phase space projection of the phase space trajectories. (a) At $r = 42$ the phase space trajectories fill the torus (quasiperiodic). (b) At $r = 44$ the system is in a phase-locked state, and the phase space trajectory does not fill the torus (limit cycle).

$r = 47.4$ at which point another pair of Floquet multiplier again crosses the unit circle in a forward NS bifurcation (see Fig. 5(d)) giving rise to a quasi-periodic state. In the periodic window the largest Floquet multiplier is 1 as illustrated by the 'BC' window in Fig. 4. This quasi-periodic state subsequently becomes chaotic at $r = 48.4$ that continues for higher values of r. A zoomed portion of this regime of r is shown in the upper inset of Fig. 3. We also note that the size of the chaotic attractor is much larger than the QP attractor. This feature can be explained using 'attractor-merging crisis' to be discussed below.

We discussed earlier that in the band $r = 46.2 - 48.4$ the low-dimensional model has a periodic and a quasiperiodic attractor. However, in the same band of r, a different set of initial conditions yield another attractor which is chaotic (see Fig. 10). These two attractors have been shown in Fig. 9(a), with the green region as the QP attractor and the pink region as the chaotic attractor. At $r = 48.4$ these two attractors merge through 'attractor-merging crisis' and form a single large attractor shown in Fig. 9(b). The size of the resulting attractor is much larger that the original QP attractor but similar to that of the chaotic attractor of Fig. 10.

To ascertain the chaotic nature of the solutions obtained in our low-dimensional system, we compute the Lyapunov exponents associated with the various solutions presented in

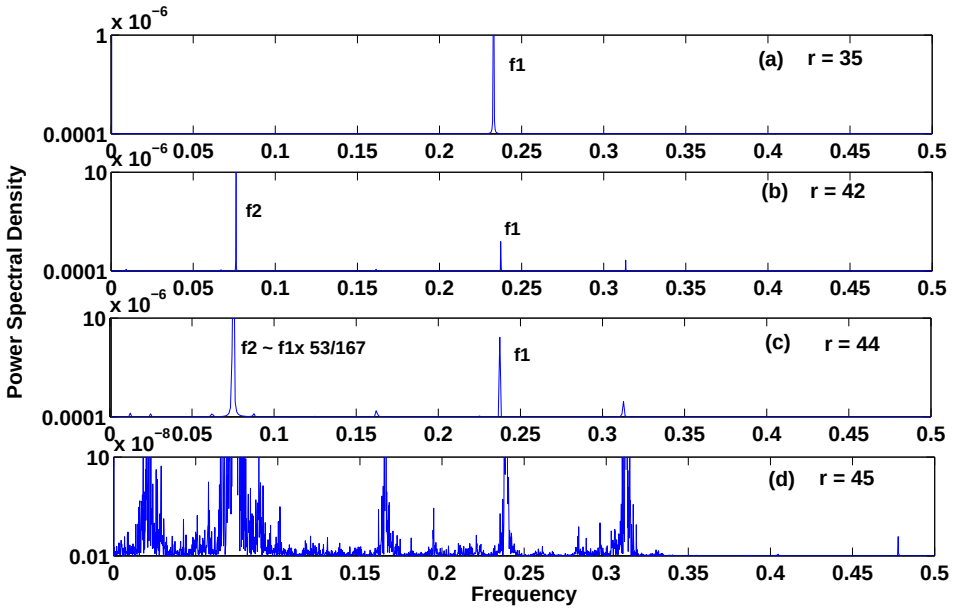

FIG. 7: The power spectral density of the mode W_{101} for various dynamical states: (a) periodic, (b) quasiperiodic ($f_1/f_2 \approx 3.099$), (c) phase locked ($f_1/f_2 \approx 3.152 \sim 167/53$), (d) chaos.

Figs. 3 and 10. The three largest Lyapunov exponents of our system corresponding to the attractors in Figs. 3 and 10 are shown in Figs. 11 and 12 respectively. There is at least one zero Lyapunov exponent throughout the range consistent with the fact that our system is autonomous. In the chaotic regions described earlier there are two positive Lyapunov exponents clearly distinct from the zero exponent ascertaining the chaotic nature of the solutions. The largest Lyapunov exponents in Fig. 11 is zero for $r = 46.2 - 48.4$ that corresponds to the periodic and quasiperiodic window shown in Fig. 3.

IV. DISCUSSIONS AND CONCLUSIONS

In this paper we present a bifurcation analysis of a 30-mode model for the Prandtl number $P = 6.8$ (a typical large-Prandtl number fluid) and aspect ration $2\sqrt{2}$. In our bifurcation analysis we observe various patterns: steady rolls ($r = 1 - 27.6$), time-periodic rolls ($r = 27.6 - 40.3$), quasiperiodicity ($r = 40.3 - 43.8$), phase locking ($r = 43.8 - 44.2$), and chaos ($r > 44.2$). The route to chaos is similar to that of Curry-Yorke model [31] where chaos occurs after quasiperiodicity and phase locking. Periodic and quasiperiodic rolls reappear

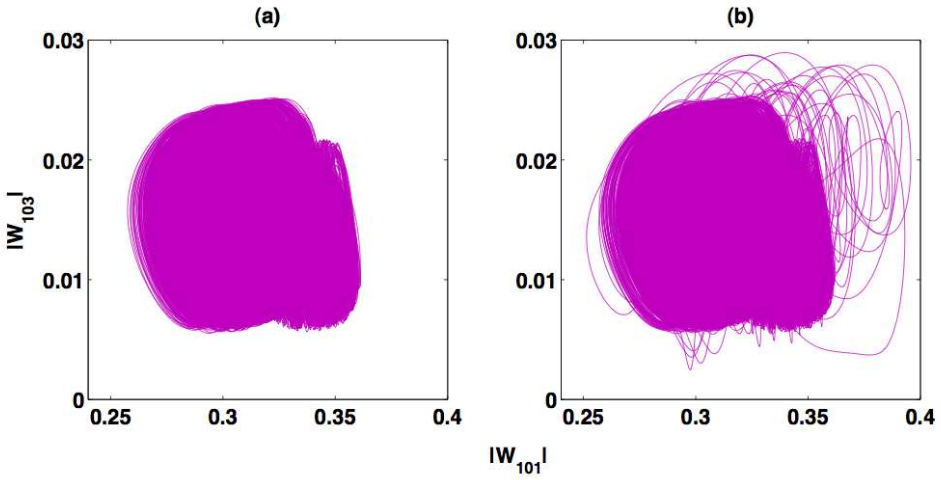

FIG. 8: The phase space projection on the $|W_{101}| - |W_{103}|$ plane of the chaotic attractor at (a) $r = 45.8$ and (b) 45.9. The chaotic attractor shows a sudden increase in size at $r = 45.9$.

after the chaotic state in the range of $r = 46.2 - 47.4$ and $r = 47.4 - 48.4$ respectively. After the second quasiperiodic window the system becomes chaotic again through 'crisis'. A distinct feature of our low-dimensional model is that we track the fixed points, limit cycles, and chaotic attractors, thus getting a detailed bifurcation picture for the range of r under investigation.

The above features of our 30-mode model closely resemble some of the past experimental results on large-Prandtl number convection namely that of Gollub and Benson [10] who observed chaos in water for various Prandtl numbers and aspect ratios. The route to chaos in Gollub and Benson's experiment for $P = 5$ and aspect ratio of 3.5 is through quasiperiodicity and phase locking. In direct numerical simulation of 3D RBC, Curry *et al.* [20] and Yahata [21] observed similar transition to chaos for $P = 10$ and $P = 5$ respectively. Our low-dimensional model follow the same route to chaos. The range of Rayleigh numbers for our low-dimensional model is quite close to the Gollub and Benson's experiments and Curry *et al.*'s and Yahata's DNS. Thus our low-dimensional model appears to capture the dynamics of 3D RBC responsible for transition to chaos through quasiperiodicity and phase locking.

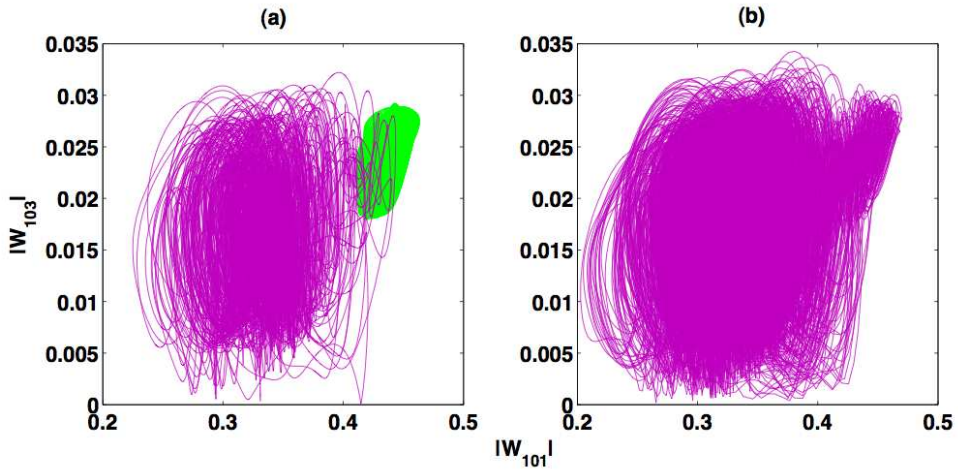

FIG. 9: The phase space projection on the $|W_{101}| - |W_{103}|$ plane at (a) $r = 48.3$ and (b) 48.5. (a) At $r = 48.3$, two attractors, a chaotic attractor (pink patch) and a quasi-periodic attractor (green patch) coexist. These two attractors are accessible through two different initial conditions. (b) At $r = 48.5$ the two attractor merges to generate a larger chaotic attractor.

Our low-dimensional model also exhibits coexistence of several attractors. In the window of $r = 46.2 - 48.4$, the system has periodic and quasiperiodic attractor along with a chaotic attractor. Coexistence of patterns and different attractors have been observed earlier [32]. Another novel feature of our low-dimensional model is that it reproduces reappearance of periodic rolls after chaos, a feature observed in the 2D DNS of Curry *et al.* [20] and Paul *et al.* [26], albeit at a much different r value. This feature appears to be due to the delay of secondary instabilities in 2D DNS compared to 3D DNS.

Gollub and Benson [10] also reported chaos in their large-Prandl number RBC through period-doubling, generation of three frequency (quasiperiodicity), and intermittency for different sets of Prandtl numbers and aspect ratios. Our preliminary investigation for $P = 10$ and aspect ratio of $2\sqrt{2}$ appears to indicate intermittency, however, we need to study this phenomena more carefully. Some of the features reported by Gollub and Benson could possibly be captured by our model by varying the aspect ratio, a topic to be investigated in future. Further work is required in construction and analysis of more refined models for

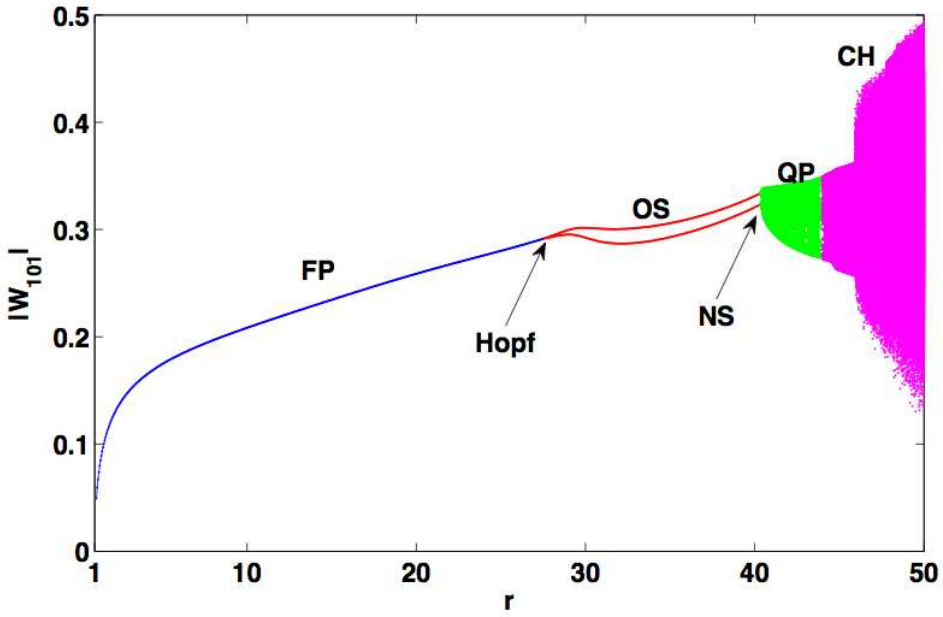

FIG. 10: Bifurcation diagram for the low-dimensional model with initial condition different from the one used for generating Fig. 3. 'FP' stands for fixed point state (blue), 'OS' stands for oscillatory state (red), 'QP' stands for quasi-periodic state (green) and 'CH' stands for chaotic state (pink). 'NS' stands for the Neimark-Sacker bifurcation point. The present attractor and that of Fig. 3 differ for $r = 46.2 - 48.4$.

RBC.

Acknowledgments

We thank Krishna Kumar, Pankaj Mishra, and Pinaki Pal for useful discussion. Part of this work is supported by the grant of Swarnajayanti fellowship to MKV by Department of Science and Technology, India. Our model is motivated by DNS runs performed in EKA of Computational Research Laboratory (CRL), Pune. We thank CRL for providing us access to EKA.

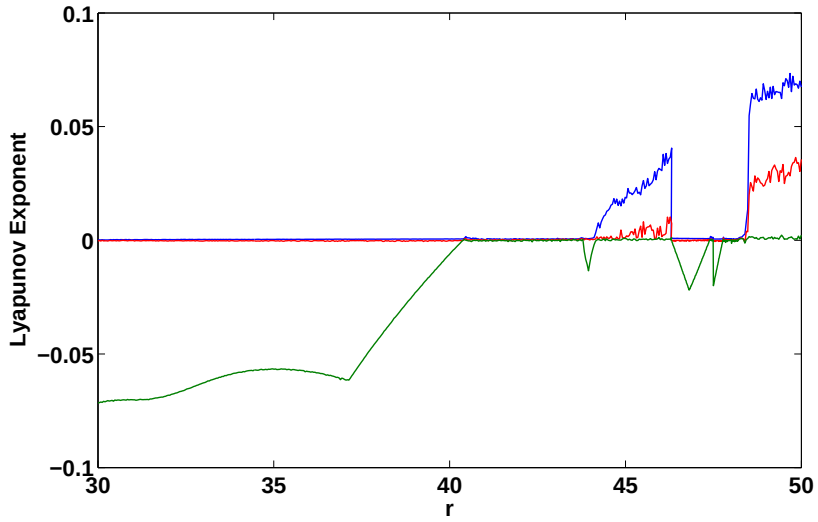

FIG. 11: Three largest Lyapunov exponents of the low-dimensional model corresponding to the attractors in Fig. 3.

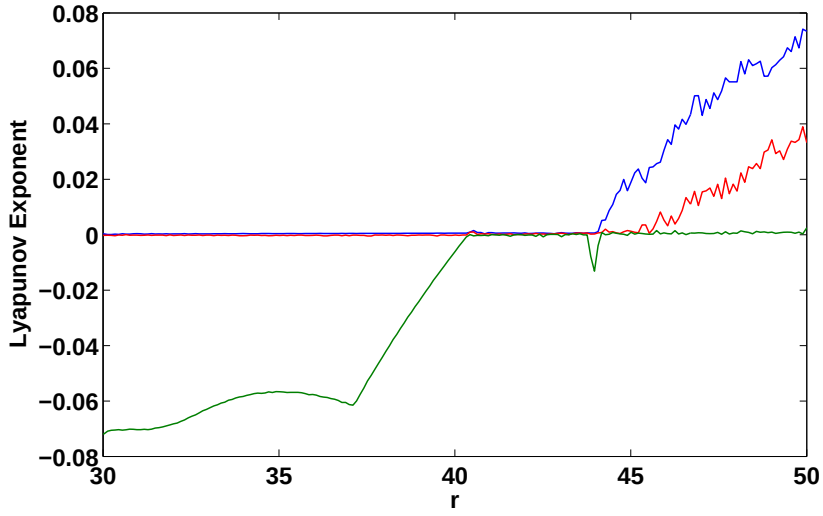

FIG. 12: Three largest Lyapunov exponents of the low-dimensional model corresponding to the attractors in Fig. 10.

APPENDIX A: NUMERICAL SEARCH FOR PERIODIC SOLUTIONS OF UNKNOWN PERIODS THROUGH FIXED POINTS OF A MAP

Consider a system of first order autonomous ODEs given by

$$\dot{\vec{x}} + \vec{f}(\alpha, \vec{x}) = 0\,, \tag{A1}$$

where, $\vec{x} \in \mathbb{R}^n$, α is a parameter and $\vec{f}(\alpha, \vec{x})$ is a known vector valued function and is such that Eq. (A1) has a periodic solution. For each value of the parameter α, we seek the initial conditions $\vec{A}$ corresponding to a periodic solution and the time period T of the periodic solution. Hence, if we numerically integrate the above equation, i.e., Eq. A1) with $\vec{x}(0) = \vec{A}$ till time T, we should have

$$\vec{x}(T) - \vec{A} \,=\, 0\,. \tag{A2}$$

Equation (A2) gives us n algebraic equations. However, we have $n+1$ unknowns, viz. the n components of $\vec{A}$ and the time-period of the periodic solution T, and hence, we require one more equation. This equation is obtained by putting a constraint that the initial condition $\vec{A}$ correspond to the extremum of one of the components, e.g., x_1. Accordingly, we will require

$$\dot{x}_1(T) \,=\, f_1(\alpha, \vec{x}(T)) \,=\, 0\,. \tag{A3}$$

Denoting

$$\vec{y} = \begin{pmatrix} \vec{A} \\ T \end{pmatrix},$$

we can write Eqs. (A2) and (A3) as

$$\vec{g}(\vec{y}) = 0. \tag{A4}$$

Equation (A4) can now be solved numerically using the Newton-Raphson method. Note that evaluation of g in the solution procedure involves background numerical solution of the ODEs (Eq. (A1)). This numerical integration can be avoided if an analytical solution were available for the ODEs such that the map $\vec{g}$ would be known analytically. However, the basic principle of constructing the map $\vec{y} = \vec{g}(\vec{y})$ whose fixed points gives us the appropriate initial conditions and the time-period of the unknown periodic solution of the ODEs remains

the same.

---

[1] S. Chandrasekhar, *Hydrodynamic and Hydromagnetic Stability* (Cambridge University Press, Cambridge, 1961); F. H. Busse, in *Hydrodynamic Instabilities and the Transition to Turbulence*, edited by H. L. Swinney, J. P. Gollub, Topics in Appl. Phys., **45** (Springer, Berlin, 1985), pp. 97 - 137; J. K. Bhattacharjee, *Convection and Chaos in Fluids*, (World Scientific, Singapore, 1987); E. Bodenschatz, W. Pesch, G. Ahlers, "Recent developments in Rayleigh-Bénard convection" *Annu. Rev. Fluid Mech.*, **32**, 709 (2000); P. Manneville, *Instabilities, Chaos and Turbulence*, (Imperial College Press, London, 2004).

[2] A. Schlütter, D. Lortz, F. H. Busse, "On the stability of steady finite amplitude convection", *J. Fluid Mech.* **23**, 129 (1965).

[3] F. H. Busse, J. A. Whitehead, "Instabilities of convection rolls in a high Prandtl number fluid", *J. Fluid Mech.* **47**, 305 (1971).

[4] F. H. Busse, "Non-linear properties of thermal convection"*Rep. Prog. Phys.* **41**, 1929 (1978).

[5] F. H. Busse, R. M. Clever, "Instabilities of convection rolls in a fluid of moderate Prandtl number"*J. Fluid Mech.* **91**, 319 (1979).

[6] M. C. Cross and P. C. Hohenberg, *Rev. Mod. Phys.* bf 65, 851(1993). G. Ahlers, in *25 Years of Nonequilibrium Statistical Mechanics*, edited by J. J. Brey, J. Marro, J. M. Rubí and M. S. Miguel,Lecture Notes in Physics, (Springer, Berlin, 1995), pp. 91-124.

[7] A. Libchaber, C. Laroche, S. Fauve,"Period doubling cascade in mercury, a quantitative measurement", *J. Physique Lett.*, **43**, L211 (1982); A. Libchaber, S. Fauve, C. Laroche,"Two-parameter study of the routes to chaos", *Physica D*, **7D**, 73 (1983).

[8] M. Giglio, S. Musazzi, U. Perini, "Transition to Chaotic Behavior via a Reproducible Sequence of Period-Doubling Bifurcations", *Phys. Rev. Lett* **47**, 243 (1981).

[9] P. Bergé, M. Dubois, P. Manneville, Y. Pomeau, "Intermittency in Rayleigh-Bénard convection", *J. Physique Lett.* **41**, L341 (1980).

[10] J. P. Gollub, S. V. Benson, "Many routes to turbulent convection" *J. Fluid Mech.* **100**, 449 (1980).

[11] J. Stavans, F. Heslot, A. Libchaber, "Fixed winding number and the quasiperiodic route to chaos in a convective fluid", *Phys. Rev. Lett.* **55**, 596 (1985).

[12] F. H. Busse, "The oscillatory instability of convection rolls in a low Prandtl number fluid", *J. Fluid Mech.* **52**, 97 (1972); M. R. E. Proctor, "Inertial convection at low Prandtl number", *J. Fluid Mech.* **82**, 97 (1977); R. M. Clever, F. H. Busse, "Low-Prandtl-number convection in a layer heated from below", *J. Fluid Mech.* **102**, 61 (1981); K. Kumar, S. Fauve, O. Thual, "Critical self-tuning: the example of zero Prandtl number convection", *J. Phys. II (France)* **6**, 945 (1996).

[13] P. Pal, P. Wahi, M. K. Verma, S. Paul, K. Kumar, P. K. Mishra, "Bifurcation and chaos in zero Prandtl number convection", to appear in *Europhys. Lett.*, arXiv:0905.4265v1.

[14] A. P. Vincent, D. A. Yuen, "Transition to turbulent thermal convection beyond $Ra = 10^{10}$ detected in numerical simulations" *Phys. Rev. E* **61**, 5241 (2000).

[15] J. Schmalzl, M. Breuer, U. Hansen, "On the validity of two-dimensional numerical approaches to time-dependent thermal convection", *Europhys. Lett.* **67**, 390 (2004).

[16] R. Krishnamurti, "On the transition to turbulent convection. Part 1. The transition from two- to three-dimensional flow ", *J. Fluid Mech.* **42**, 295 (1970); R. Krishnamurti, "On the transition to turbulent convection. Part 2. The transition to time-dependent flow", *J. Fluid Mech.* **42**, 309 (1970).

[17] J. Maurer, A. Libchaber, "Rayleigh-Bénard experiment in liquid helium ; frequency locking and the onset of turbulence", *J. Physique Lett.*, **40**, 419 (1979).

[18] S. Ciliberto, M. A. Rubio, "Chaos and Order in the Temperature Field of Rayleigh-Bénard Convection", *Physica Scripta* **36**, 920 (1987).

[19] S. W. Morris, E. Bodenschatz, D. S. Cannell, G. Ahlers, "Spiral defect chaos in large aspect ratio Rayleigh-Bénard convection", *Phys. Rev. Lett.* **71**, 2026 (1993).

[20] J. H. Curry, J. R. Herring, J. Loncaric, S. A. Orszag, "Order and disorder in two- and three-dimensional Bénard convection", *J. Fluid Mech.* **147**, 1 (1984).

[21] H. Yahata, "Transition to chaos in the Rayleigh-Bénard convection", *J. Phys. Soc. Jpn.* **69**, 1384(2000).

[22] D. Mukutmoni and K. T. Yang, "Rayleigh-Bénard convection in a small aspect ratio enclosure. II: Bifurcation to chaos", *J. Heat Transfer* **115**, 367(1993).

[23] D. R. Moore, N. O. Weiss, "Two-dimensional Rayleigh-Bénard convection", *J. Fluid Mech.* **58**, 289(1973).

[24] J. B. McLaughlin, S. A. Orszag, "Transition from periodic to chaotic thermal convection", *J.*

Fluid Mech. **122**, 123 (1982).

[25] I. Goldhirsch, R. B. Pelz, S. A. Orszag, "Numerical simulation of thermal convection in a two-dimensional finite box ", *J. Fluid Mech* **199**, 1 (1989).

[26] S. Paul, P. K. Mishra, M. K. Verma, K Kumar, "Order and chaos in two-dimensional Rayleigh-Bnard convection", arXiv:0904.2917v1, (2009); S. Paul, K. Kumar, M. K. Verma, D. Carati, A. De, V. Eswaran, "Chaotic traveling rolls in Rayleigh-Bénard convection", to appear in *Pramana*, (2009), arXiv:0704.3795v2 (2007).

[27] J. H. Curry, "Chaotic response to periodic modulation of model of a convecting fluid", *Phys. Rev. Lett.*, **43**, 1013 (1979).

[28] J. H. Curry, "A Generalized Lorenz System ", *Comm. Math. Phys.*, **60**, 193 (1978).

[29] H. Yahata, "Transition to turbulence in the Rayleigh-Bénard convection", *Prog. Theor. Phys.* **68**, 1070(1982).

[30] H. Yahata, "Period-doubling cascade in the Rayleigh-Bénard convection", *Prog. Theor. Phys.* **69**, 1802(1983).

[31] P. Bergé, Y. Pomeau, C. Vidal, *Order within chaos*, (John Wiley & Sons, Paris, 1984).

[32] G. Metcalfe, R. P. Behringer, "Convection in ^{3}He-superfluid-^{4}He mixtures. Part 2. A survey of instabilities", *J. Fluid Mech.*, **307**, 297 (1996).